

Neuron, Volume 90

Supplemental Information

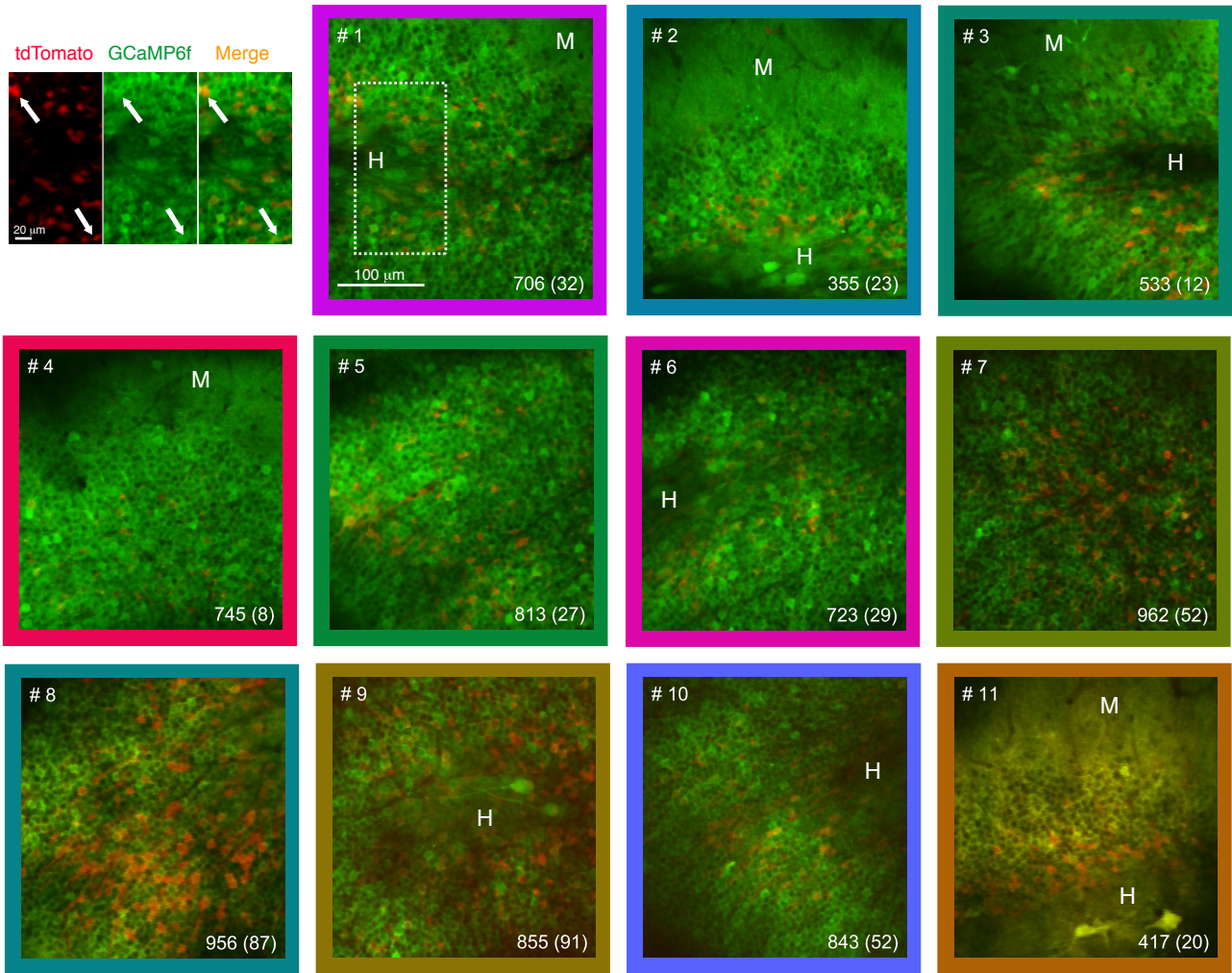
Distinct Contribution of Adult-Born

Hippocampal Granule Cells to Context Encoding

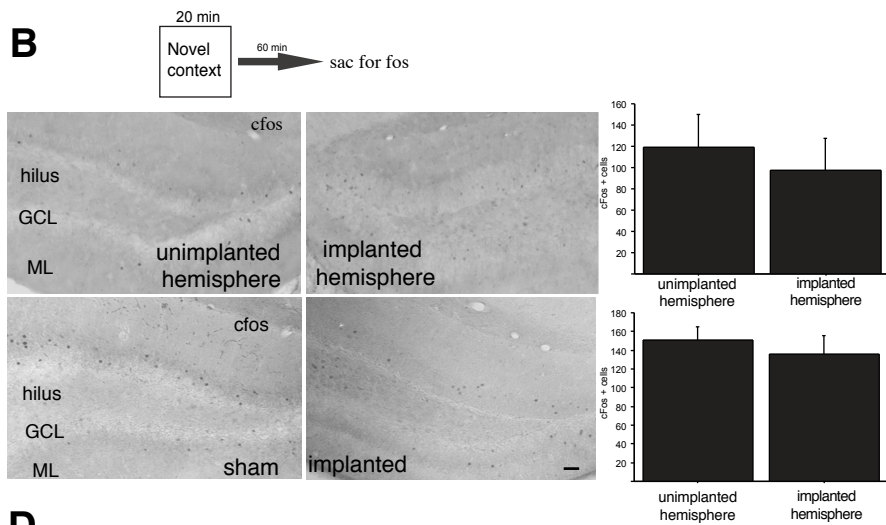
Nathan B. Danielson, Patrick Kaifosh, Jeffrey D. Zaremba, Matthew Lovett-Barron, Joseph Tsai, Christine A. Denny, Elizabeth M. Balough, Alexander R. Goldberg, Liam J. Drew, René Hen, Attila Losonczy, and Mazen A. Kheirbek

Supplemental figure 1

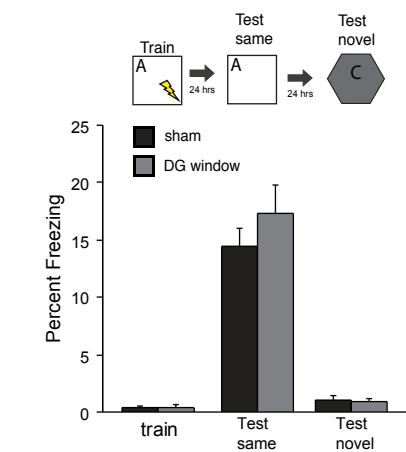
A



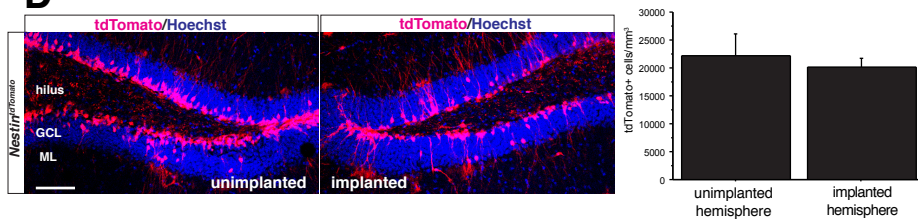
B



C



D



E

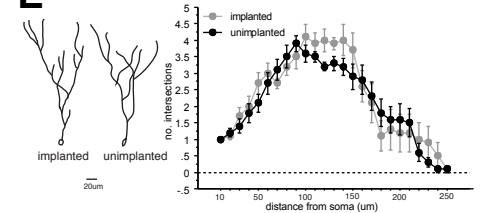


Figure S1, related to Figure 1: *In vivo* Ca²⁺ imaging of DG GCs

(a) Images of all fields of view during 2P DG imaging. The FOV from which the example cells in Fig. 2A,B were drawn. Arrows mark the location of the example newborn (tdTomato-positive) and mature (tdTomato-negative) cell. The corresponding area is shown in FOV #1. The numbers in each FOV indicate the number of mGCs (719 ± 204 , mean \pm s.d., $n = 11$ FOVs) and abGCs (39 ± 28 , mean \pm s.d., $n = 11$ FOVs) identified. The border color around each FOV matches the color scheme used through the figures. In some fields the two-photon imaging plane passes through the hilar (*H*) or molecular layers (*M*) as a consequence of the curved 3D geometry of the dentate gyrus dorsal blade **(b-c)** Window implantation does not impact overall DG activity or hippocampus-dependent contextual fear conditioning. **(b)** Implanted mice explored a novel context for 20 min and were sacrificed for cFos immunohistochemistry 60 minutes later. The number of cFos+ cells in the GCL did not differ between the implanted and unimplanted hemisphere ($n=4$, unpaired t-test, $t_6=-0.5$, $p=0.64$). In addition, cFos+ cells did not differ between implanted and sham mice $n=3-4$ /condition, unpaired t-test, $t_5=-0.6$, $p=0.57$) (scale bar=100um). **(c)** Window implantation did not impact one-trial contextual fear conditioning ($n=8$ sham, 7 DG window, group effect $F_{(1,13)}=0.9$, $p=0.36$, training effect $F_{(1,13)}=113.9$, $p<0.001$ group X training interaction $F_{(1,13)}= 0.93$, $p=0.35$ (on test same context $t_{13}=-.9$, $p=0.34$). In addition, mice with window implantation could discriminate between different contexts (group effect $F_{(1,26)}=0.9$, $p=0.36$, context effect $F_{(1,26)}=1635$, $p<0.001$ group X context interaction $F_{(1,26)}= 17.3$, $p=0.32$). **(d)** Window implantation did not impact total number of six week old and younger tdTomato+ abGCs in the implanted hemisphere ($n=6$ unpaired t-test, $t_6=-0.6$, $p=0.59$). **(e)** We conducted analysis on the dendrites of abGCs in the implanted and unimplanted hemispheres, and did not detect significant differences in the dendritic architecture of neurons on the implanted side ($n=10$ /side, repeated measures ANOVA, intersection X hemisphere interaction $F_{(24,432)}= 1.2$, $p=0.23$). We also determined the number of proliferating neurons, as measured by Ki67 immunohistochemistry, and did not detect differences (data not shown; $n=4$ /group, $t_6=-2.1$, $p=0.1$).

Supplemental figure 2

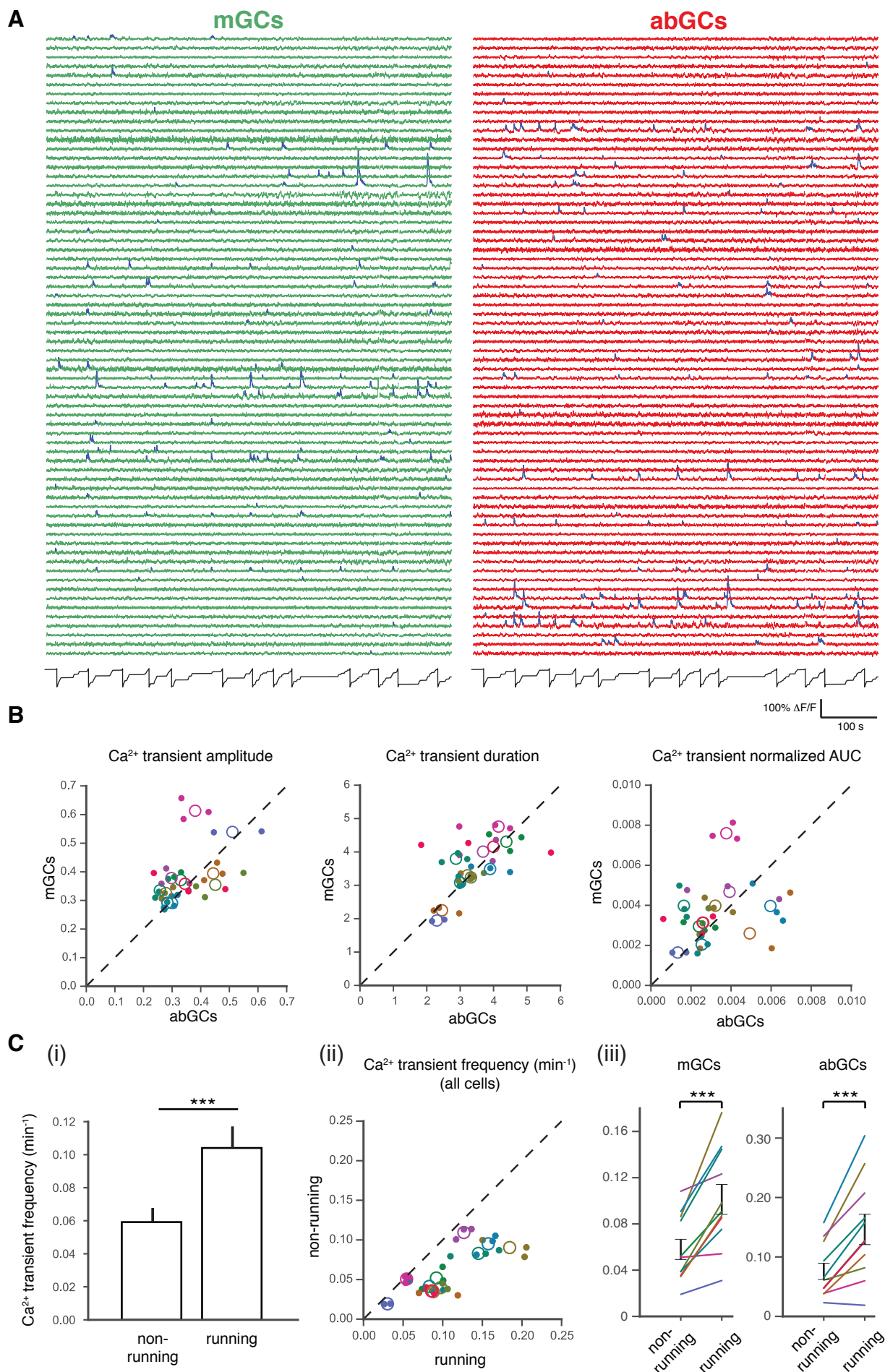


Figure S2, related to Figure 2. Population activity in DG GCs during behavior

(a) Example traces and transient detection. For a single 12-minute recording session we plotted the processed df/f Ca^{2+} trace for all newborn neurons in the FOV and for an equal number of randomly sampled mGCs. Statistically significant Ca^{2+} transients ($p < 0.05$) are indicated in blue, and the mouse's position in this experiment is plotted in black at bottom. **(b)** Activity comparison plots. As plotted in Fig 1D, for all cells imaged we computed the mean amplitude, duration, and transient AUC (total area under DF/F curve during significant transients) across recordings. Data is plotted by averaging mature and newborn subpopulations across experiments (closed circles) and FOVs (open circles). Across FOVs and cells, we did not detect differences between mGCs and abGCs in the amplitude or duration of calcium transients (2-sample paired T-Test; $n=11$ FOV; $p=0.21, 0.45,$ and 0.42 for amplitude, duration, and transient AUC, respectively). **(c)** Non-running vs. running analysis. *(i)* Mean Ca^{2+} transient frequency with onset during non-running and running-related imaging frames. Across fields of view, running-related transients are observed at a significantly higher rate during running than during non-running epochs (non-running: 0.06 ± 0.01 transients/min.; running: 0.10 ± 0.01 transients/min.; $t=-5.66$; $p<0.001$; $n=10$ FOV; paired T-Test). *(ii)* Scatter of mean running-related and non-running-related Ca^{2+} transient frequency by recording (closed circles) and by FOV (open circles). Color as in Fig S1. *(iii)* Data aggregated by FOV separately for mGCs and for abGCs. Both populations showed higher activity during running than non-running periods (mGCs: non-running: 0.06 ± 0.01 transients/min.; running: 0.10 ± 0.01 transients/min.; $t=-5.60$; $p<0.001$; $n=11$ FOV; paired T-Test; abGCs: non-running: 0.08 ± 0.01 transients/min.; running: 0.15 ± 0.03 transients/min.; $t=-5.16$; $p<0.001$; $n=11$ FOV; paired T-Test).

Supplemental figure 3

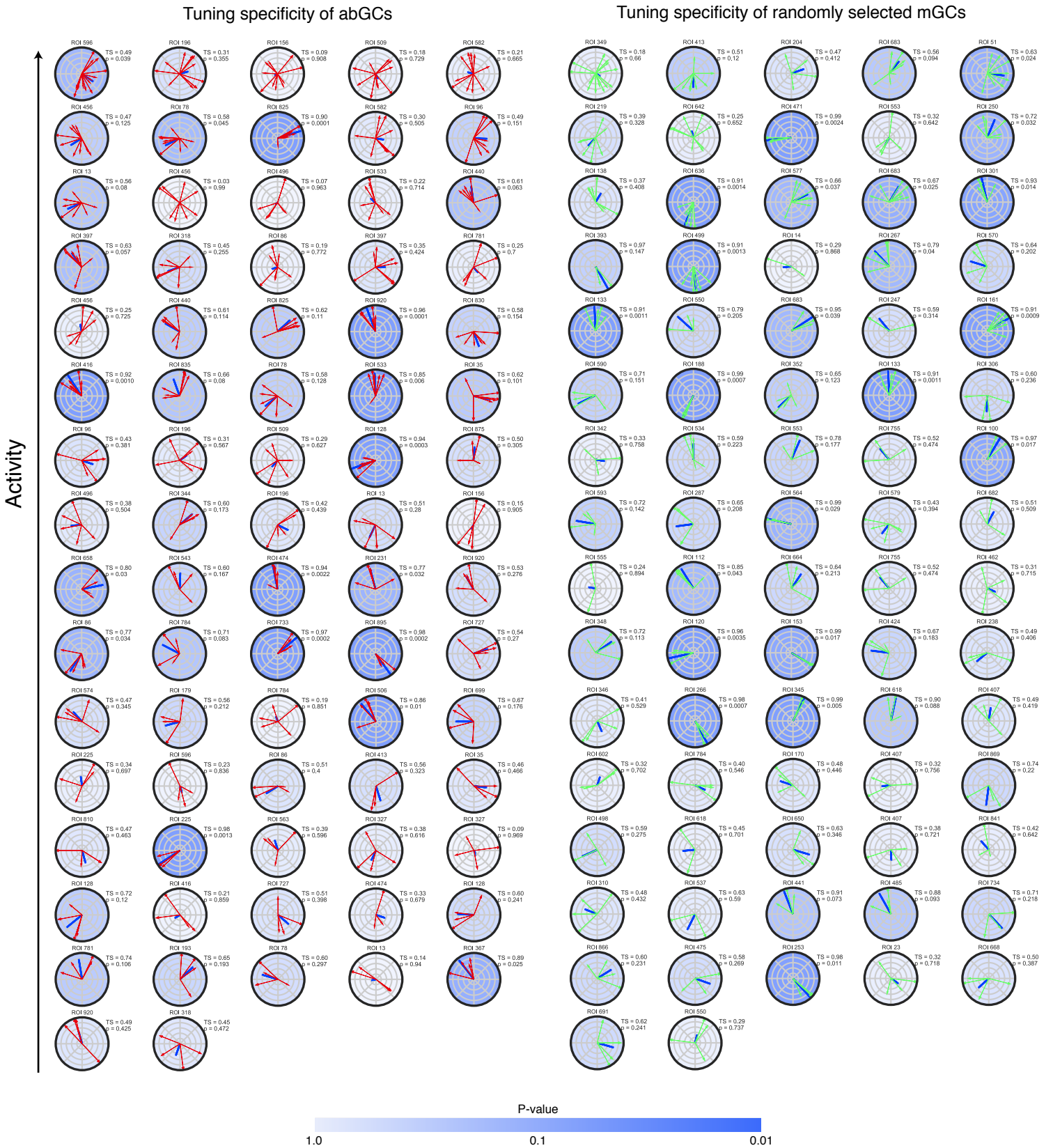


Figure S3, related to Figure 2. Tuning direction plots of abGCs and mGCs

For every abGC firing at least four significant transients, we plotted the direction of every running-related transient as well as the overall tuning direction (dark blue line). Vectors are inversely weighted by occupancy and normalized to peak. Tuning strength (*TS*) and associated p-value is indicated for each cell. P-values are calculated relative to the expected distribution for an equal number of running-related transients randomly distributed in time (see Methods). The blue background shading is a reflection of the tuning specificity p-value. Color intensity is logarithmically related to the p-value. B) For random sampled mature granule cells firing with least four significant transients, we plotted the direction of every running-related transient as well as the overall tuning direction (dark blue line). Vectors are inversely weighted by occupancy and normalized to peak. Tuning strength (*TS*) and associated p-value is indicated for each cell. P-values are calculated relative to the expected distribution for an equal number of running-related transients randomly distributed in time (see Methods). The blue background shading is a reflection of the tuning specificity p-value. Color intensity is logarithmically related to the p-value.

Supplemental figure 4

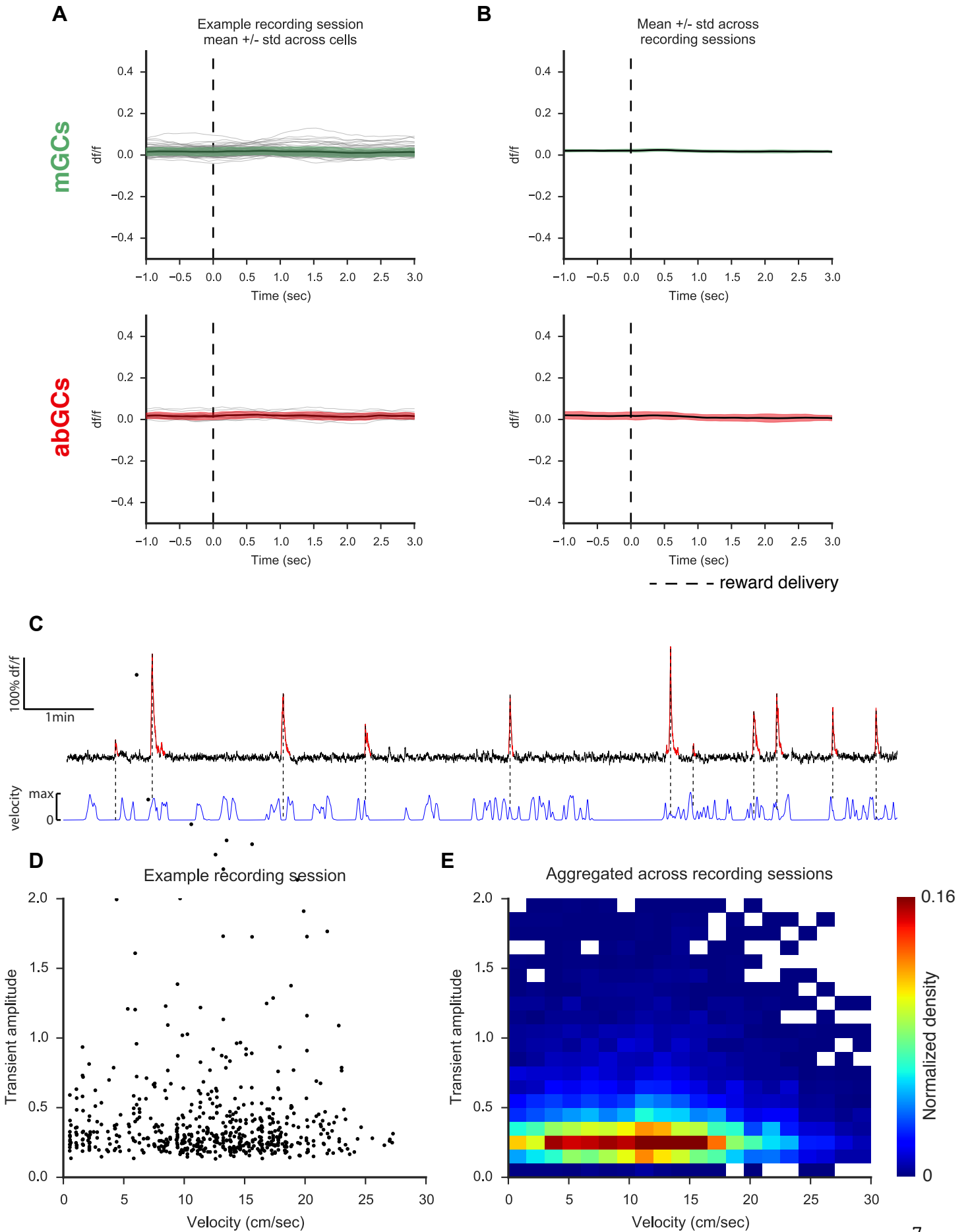


Figure S4, related to Figure 2. Reward and velocity-related responses

(a-b) For each cell we calculated a peri-stimulus time histogram (PSTH) for GCaMP6f fluorescence triggered on the delivery of the water rewards. Because so many of the granule cells are silent, we included only active cells in this analysis (at least 4 Ca^{2+} transients). **(a)** Data from active cells in a single experiment. mGCs and abGCs are on top and bottom respectively. Light gray traces reflect the PSTH's of individual cells in the recording (n=92 mGCs, n=13 abGCs). Shaded region is the mean +/- the standard deviation of the Ca^{2+} responses. Three randomly placed rewards were administered per lap. PSTHs are based on all reward presentations in the experiment. **(b)** Mean +/- the standard deviation of the means for each recording session (n=32 recordings). In none of our recordings did we find a significant reward response. **(c-d)** In order to determine if activity is related to velocity, it is necessary to estimate a continuous firing rate, which can then be correlated with the animal's velocity (Kropff et al., 2015). Estimating a continuous firing rate from calcium imaging data is difficult, however, and is not possible in context of very low transient rates, as were observed in this study. The best proxy we have for spike rate is the amplitude of the detected transients (large transients reflect large bursts of spikes, while small transients reflect fewer numbers of spikes). If there were a relationship between activity and velocity, then large amplitude events should be associated with faster velocities and vice versa. For this analysis we included only transients associated with a non-zero velocity to maximize our likelihood of detecting a relationship. **(c)** Top: df/f Ca^{2+} trace from an example cell. Significant transients ($p < 0.05$) in red. Bottom: The mouse's velocity over the course of the same 10min trial. **(d)** Scatter plot of transient amplitude vs. the mouse's velocity at the time of transient onset. There was no relationship between amplitude and velocity (Pearson $r = -0.009$, $p = 0.81$). **(e)** Data was combined across all recording sessions and a 2D-histogram was calculated. Color indicates the density of transients in each bin. Upper and lower colormap values represent the 1st and 99th percentiles of the density distribution.

e

Supplemental figure 5

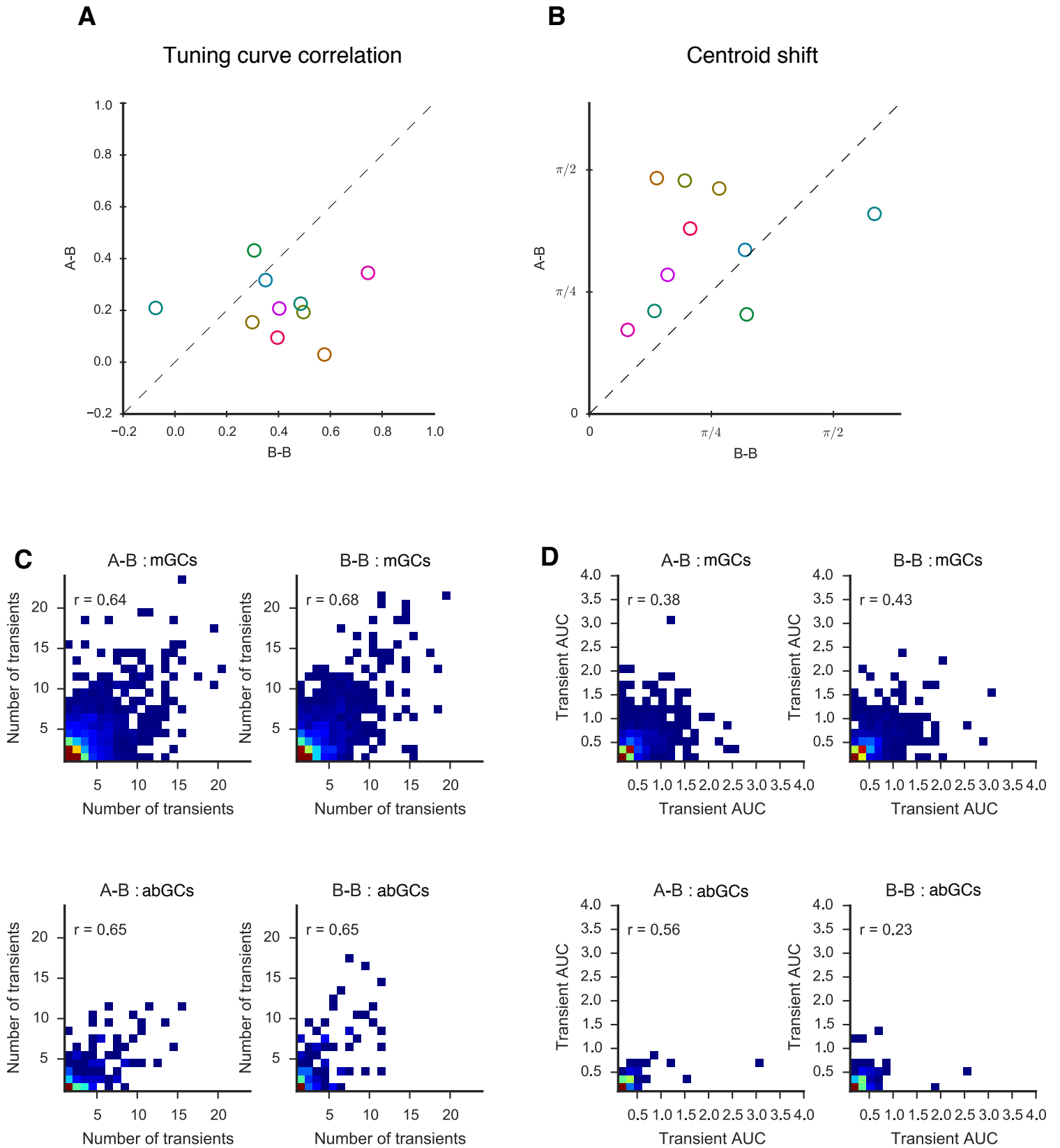


Figure S5, related to Figures 3-5. Remapping dynamics

Tuning curve correlations (**a**) and centroid shift (**b**) assessed by averaging across mGCs within each FOV. mGCs in 8/10 FOVs maintained significantly more similar spatial representations in the A-A condition than in the A-B condition (paired two-sided T-Test; $n=10$, **b**, $T_{(18)} = 2.27$, $p < 0.05$; **c**, $T_{(18)} = -1.97$, $p = 0.07$). (**c-d**) In order to assess encoding of context through overall activity throughout the trial, we plotted the total number of transients (**c**) and mean transient AUC (total area under all significant transients; **d**) in one trial as a function of the activity in the next trial. This two-dimensional data was binned, and a normalized 2D-histogram was calculated. Upper and lower colormap values represent the 1st and 99th percentiles of the density distribution. The relationship between trial-to-trial activity in the 'B-B' condition appears similar as that of the 'A-B' condition, supporting our analysis in **Fig 6**. Data is plotted separately for newborn (*bottom*) and mature (*top*) cells and for the 'A-B' (*left*) and 'B-B' (*right*) conditions.

Supplemental figure 6

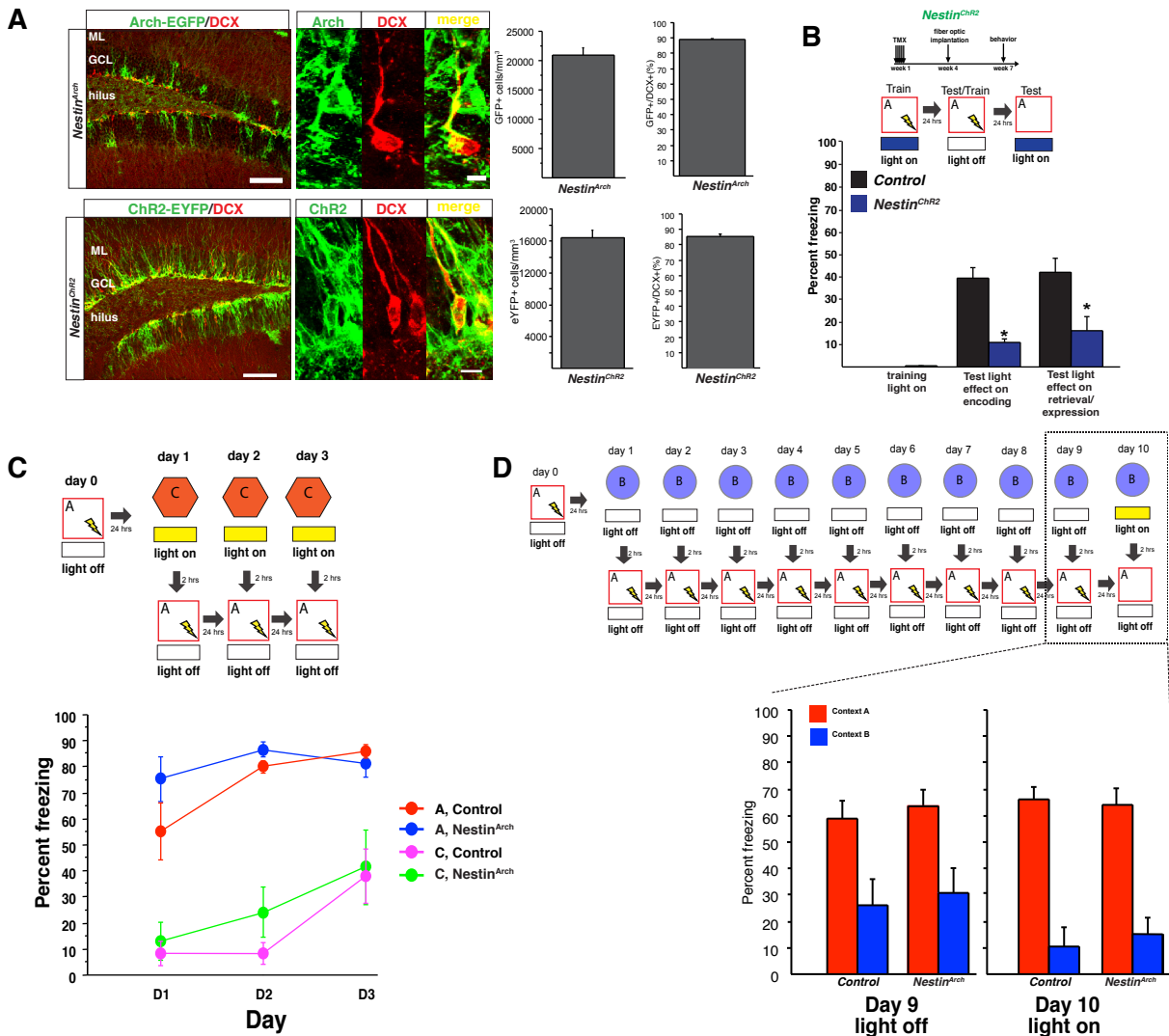


Figure S6, related to Figure 6. Optogenetic modulation of abGCs.

(a) Expression of opsins in abGCs. TMX induction was performed as described in the Methods. In the DG of *Nestin^{Arch}* and *Nestin^{Chr2}* mice, the majority of DCX+ cells expressed opsins (n=3-4/geno *Nestin^{Arch}*: 88.9 +/- 2.9%, n=3-4/geno, *Nestin^{Chr2}*: 85.4 +/- 2.9% of the DCX population of immature cells). (Scale bars 100um (low mag) and 10um (high mag)) **(b)** Stimulation of abGCs in the dorsal DG impairs encoding and retrieval of fear memories (n=9 control, 8 *Nestin^{Chr2}*, group effect $F_{(1,15)}=11.12$, $p=0.005$, group X training interaction $F_{(1,14)}=24.4$, $p=0.0064$ (on test off day $t_{14}=5$, $p<0.01$, on test on day $t_{14}=2.9$, $p=0.01$). **(c)** Inhibition of abGCs during exposure to a highly dissimilar context does not impair discrimination. (n=5 control, 4 *Nestin^{Arch}*, group effect $F_{(1,14)}=1.5$, $p=0.23$, context effect $F_{(1,14)}=78.9$, $p<0.001$, day effect $F_{(2,28)}=17.4$, $p<0.001$, groupXdayXcontext effect $F_{(2,28)}=1.5$, $p=0.24$.) This ability to discriminate may also be due to the fact that young neurons were not required to associate the tactile cues of the bars with the delivery of the footshock. **(d)** Inhibition of abGCs does not impair the expression of contextual fear discrimination. Mice were trained to discriminate between two similar contexts then tested for light effects in the similar context after the discrimination had already been learned. *Nestin^{Arch}* and control mice learned the discrimination task in the absence of light stimulation indicating that TMX or gene expression does not impact discrimination learning (n=7 control 8 *Nestin^{Arch}*, group effect $F_{(1,26)}=3.5$, $p=0.1$, context effect $F_{(1,26)}=10.2$, $p=0.004$, day effect $F_{(8,208)}=15.2$, $p<0.001$, groupXdayXcontext effect $F_{(8,208)}=0.1$, $p=0.52$. Control: context effect $F_{(1,12)}=4.8$, $p=0.02$, dayXcontext interaction $F_{(8,96)}=2.2$, $p<0.01$. *Nestin^{Arch}*: context effect $F_{(1,14)}=5.9$, $p=0.04$, day X context effect $F_{(8,112)}=2.1$, $p=0.04$). Yellow light inhibition did not impact fear discrimination (repeated measures ANOVA, group effect $F_{(1,26)}=.2$, $p=0.64$, context effect $F_{(1,26)}=43.9$, $p<0.001$, group X context interaction $F_{(1,26)}=0.1$, $p=0.8$, group X context X day $F_{(1,26)}=0.3$, $p=0.59$. Error bars are mean +/- SEM

<i>cohort</i>	<i>implant location</i>	<i>test</i>	<i>conditions</i>	<i>stats</i>
Nestin Arch	dorsal DG	shock reactivity	0.75 mA shock	n=8-9/treatment, $t_{15}=0.9$, $p=0.4$
Nestin Arch	ventral DG	CFC	Light on encoding, light off test, retrain light off, test retrieval light on	n=8-11/treatment, treatment effect $F_{(1,17)}=0.56$, $p=0.46$, treatment X training interaction $F_{(1,17)}=0.46$, $p=0.5$ (on test off day $t_{17}=-0.72$, $p=0.48$, on test on day $t_{17}=-0.75$, $p=0.46$)
Nestin Chr2	ventral DG	CFC	Light on encoding, light off test, retrain light off, test retrieval light on	n=8-10/treatment., treatment effect $F_{(1,16)}=2.4$, $p=0.14$, treatment X training interaction $F_{(1,16)}=2.2$, $p=0.2$ (on test off day $t_{16}=-1.5$, $p=0.15$, on test on day $t_{16}=-0.15$, $p=0.9$)
Nestin Arch	dorsal DG	OFT	5min light off, 5min light on, 5min light off	n=8-9/ geno, total distance traveled, genotype effect $F_{(1,15)}=1.3$, $p=0.1$, genoXlight effect $F_{(2,30)}=0.4$, $p=0.7$, percent center distance: genotype effect $F_{(1,15)}=0.9$, $p=0.4$, genoXlight effect $F_{(2,30)}=2.3$, $p=0.1$
Nestin Arch	dorsal DG	EPM	5min light off, 5min light on, 5min light off	n=8/geno, total distance traveled genotype effect $F_{(1,14)}=0.4$, $p=0.6$, genoXlight effect $F_{(2,28)}=1.2$, $p=0.3$; time in open arms genotype effect $F_{(1,14)}=1.3$, $p=0.3$, genoXlight effect $F_{(2,28)}=1.8$, $p=0.2$.
Nestin Arch	ventral DG	OFT	5min light off, 5min light on, 5min light off	n=8-11/geno, total distance traveled (genotype effect $F_{(1,17)}=1.7$, $p=0.2$, genoXlight effect $F_{(2,34)}=1.2$, $p=0.3$, percent center distance: genotype effect $F_{(1,17)}=0.3$, $p=0.6$, genoXlight effect $F_{(2,34)}=0.6$, $p=0.5$
Nestin Arch	ventral DG	EPM	5min light off, 5min light on, 5min light off	n=8-9/geno, total distance traveled genotype effect $F_{(1,15)}=4$, $p=0.06$, genoXlight effect $F_{(2,30)}=0.3$, $p=0.8$; time in open arms, genotype effect $F_{(1,15)}=1.2$, $p=0.3$, genoXlight effect $F_{(2,30)}=1.2$, $p=0.3$.
Nestin Chr2	dorsal DG	OFT	5min light off, 5min light on, 5min light off	n=7-9/ geno, total distance traveled, genotype effect $F_{(1,14)}=1.1$, $p=0.3$, genoXlight effect $F_{(2,28)}=3.3$, $p=0.05$, percent center distance: genotype effect $F_{(1,14)}=0.5$, $p=0.5$, genoXlight effect $F_{(2,28)}=2.3$, $p=0.1$
Nestin Chr2	dorsal DG	EPM	5min light off, 5min light on, 5min light off	n=7-8/geno, total distance traveled genotype effect $F_{(1,13)}=0.7$, $p=0.4$, genoXlight effect $F_{(2,26)}=4.8$, $p=0.02$, time in open arms, genotype effect $F_{(1,13)}=0.4$, $p=0.6$, genoXlight effect $F_{(2,26)}=0.6$, $p=0.6$.
Nestin Chr2	ventral DG	OFT	5min light off, 5min light on, 5min light off	n=9-10/geno, total distance traveled, genotype effect $F_{(1,17)}=1.1$, $p=0.3$, genoXlight effect $F_{(2,34)}=0.4$, $p=0.7$, percent center distance: genotype effect $F_{(1,17)}=0.9$, $p=0.3$, genoXlight effect $F_{(2,34)}=0.1$, $p=0.9$
Nestin Chr2	ventral DG	EPM	5min light off, 5min light on, 5min light off	n=9-10/geno, total distance traveled genotype effect $F_{(1,17)}=1.8$, $p=0.2$, genoXlight effect $F_{(2,34)}=1.5$, $p=0.2$; time in open arms, genotype effect $F_{(1,17)}=0.3$, $p=0.6$, genoXlight effect $F_{(2,34)}=0.8$, $p=0.5$,

Table S1, related to Figure 6. Control behavioral experiments. Table contains results from behavioral experiments for effects of inhibition or excitation of abGCs in anxiety-like behavior, shock reactivity and contextual fear conditioning. (CFC- contextual fear conditioning, OFT- Open Field Test, EPM- Elevated Plus Maze)

Movie S1, related to Figure 1. Sparse granule cell population activity. 5 minutes of GCaMP6f activity in the behaving mouse (300 x 300 μm FOV, ~ 1000 cells) played at 10x speed (30sec total). Frames were smoothed with $\sigma=3$ pixels, compressed as MPEG, and edited in iMovie. Transients are observed at extremely low rates (see **Fig 2**).

Supplemental Experimental Procedures

Mice:

All experiments were conducted in accordance with the US National Institutes of Health guidelines and with the approval of the Columbia University and New York State Psychiatric Institute Institutional Animal Care and Use Committees.

Male *ROSA26-CAG-stop^{fllox}-ChR2(H134R)-eYFP (Ai32)*, *ROSA26-CAG-stop^{fllox}-Arch-GFP (Ai35)*, *ROSA26-CAG-stop^{fllox}-tDTomato (Ai9)* and Nestin-CreER^{T2} (Dranovsky et al., 2011; Madisen et al., 2012; Madisen et al., 2010) and controls were generated as previously described (on mixed background). Mice were housed in the vivarium on a 12-h light/dark cycle and were housed 3-5 mice in each cage (with genotypes/treatments randomized in each cage). Experiments were performed during the light portion of the cycle.

Imaging window implant:

Recombinant adeno-associated viruses carrying the GCaMP6f gene were obtained from the Penn Vector Core (AAV1.Syn.GCaMP6f.WPRE.SV40) with titer of $2-4 \times 10^{13}$. The dorsal dentate gyrus was stereotactically injected with 3-fold diluted virus (in artificial CSF) using a Nanoject syringe, as described in previously (Kaifosh et al., 2013; Lovett-Barron et al., 2014). Injection coordinates were -1.5 mm AP, -2.3 mm ML, and -1.8, -1.65, -1.5 mm DV relative to the cortical surface. 60 nL of diluted virus was injected at each DV location in 10 nL increments. Mice were then surgically implanted with an imaging window (diameter: 1.5-mm; height: 2.2-mm) over the left dorsal dentate gyrus and implanted with a stainless-steel headpost for head fixation during imaging experiments. Imaging cannulas were constructed by adhering (Narland optical adhesive) a 3-mm glass coverslip (64-0720, Warner) to a cylindrical steel cannula (1.5-mm diameter x 2.3-mm height) and polishing down the overhanging glass with a diamond file. We used a modified version of the same headpost described previously (Kaifosh et al., 2013; Lovett-Barron et al., 2014), in which the posterior bar was thinned to accommodate the 3.5mm working distance of the objective. The surgical procedure was very similar to that previously described, except that the imaging window was implanted 100-200 μ m above the hippocampal fissure, providing optical access to the granule cells in the dorsal blade of the DG. Following induction of anesthesia (Isoflurane: 3% induction, 1.5-2.0% maintenance; 1.0 L/min O₂) and administration of analgesia (buprenorphine 0.05-0.1 mg/kg), the scalp was removed, and a 1.5 mm diameter craniotomy was performed with a fine-tipped dental drill (V00033, Henry-Schein). The dura was removed, and the underlying cortex was aspirated to reveal the capsular fibers. Following this, a 30g blunt syringe (B30-50, SAI) was used to gently aspirate CA1 directly superior to the dentate until the loose fibers and vasculature of *stratum moleculare* were visible. Bleeding was controlled with a collagen gel sponge (A00063, Avitene) and continuous irrigation with aCSF. We then gently fit the cannula into the craniotomy and affixed the headpost to the skull using dental cement (675572, Dentsply). Mice were active within 15 minutes of surgery, and analgesia was continued for three days post-operatively.

Fiber optic construction and implantation.

Male mice (8 weeks of age) were surgically implanted with fiber optic cannulas at 3 weeks after TMX induction, using published protocols (Kheirbek et al., 2013), and behavioral experiments commenced >3 wks after surgery to allow for recovery. Briefly, a 200 μ m core, 0.37 numerical aperture (NA) multimode fiber (ThorLabs) was threaded through and glued with epoxy to a 230 μ m core, 1.25mm diameter zirconia multimode ferrule (Precision Fiber Products), polished and cut at ~4mm for implantation. They were then tested for light output (~80-90% light recovery) and clean scoring of the fiber, and then each implant was numbered and the percent light recovery was noted for calibration of output for behavioral experiments. For surgical implantation, mice were anesthetized with 100mg/kg ketamine and 10mg/kg xylazine, and placed in a stereotaxic frame (Kopf). Mice were implanted bilaterally with sterile, chronically dwelling optical fibers targeted to the DG (dorsal implants: +/-1mm ML -1.5mm AP, -1.7mm DV, ventral implants: +/-2.5mm ML +/-3.7mm AP, -2mm DV). Optical fibers were secured with anchoring screws and dental cement. After surgery, mice were returned to their home cage and monitored until recovery from surgery. 3 weeks after surgery, before beginning behavioral testing mice were habituated to being attached to the patch cable by handling and attaching to the cable via a zirconia sleeve, and allowed to explore a novel cage for 15 min with no light for two consecutive days.

Induction of transgene expression and immunohistochemistry.

All mice were induced at 8 weeks of age and immunohistochemical analysis was conducted 6 weeks after TMX induction. For all experiments, mice were perfused (transcardial PBS, 4% paraformaldehyde), brains postfixed, cryoprotected, and sections (35 μ m) of the entire DG were collected. Primary antibodies were: chicken anti-green fluorescent protein (chicken anti-GFP; (1:500, Abcam, goat anti-doublecortin (DCX; 1:500, Santa Cruz Biotechnology), rabbit anti-Ki67 (1:100, Vector), rabbit anti-cFos (Millipore, ABE457, 1:1000) and mouse anti-NeuN, 1:1500, Millipore) (Kheirbek et al., 2013; Kheirbek et al., 2012; Sahay et al., 2011).

For induction of transgene expression in Nestin-CreER^{T2} mice, 8 week-old male mice were injected with 3mg tamoxifen (TMX) (VEH solution of corn oil/10%ethanol) I.P./day for 5 consecutive days. Testing began 6 weeks after the last TMX induction, as described in the text. In the DG of *Nestin^{Arch}*, *Nestin^{ChR2}* and *Nestin^{tdTomato}* mice, the majority of DCX+ cells expressed ChR2 or Arch, respectively (n=3-4/geno, *Nestin^{ChR2}*: 85.4 \pm 2.9%, *Nestin^{Arch}*: 88.9 \pm 2.9%, *Nestin^{tdTomato}* 89.5 \pm 3.8% of the DCX population of immature cells).

For immunohistochemical characterization of ChR2-eYFP⁺ and Arch-GFP⁺ cells in the Nestin-CreERT2 and tdTomato+ cells in imaged mice, confocal stacks (FluoView1000; Olympus) of DG sections were taken at 40x. For characterization of ChR2-eYFP⁺ and Arch-GFP⁺ cells, six sections across the DV axis of the DG (~400um between sections) were used for sampling cell number. For characterizing tdTomato+ cells, two sections spanning the implant site were taken for each hemisphere to compare implanted vs unimplanted side. For cell counting, the total number of labeled cells were counted in the GCL of the dentate gyrus and this number was divided by the sample volume (area was measured by tracing Hoechst stained to sections using ImageJ and multiplied by section thickness (35um) to generate volume measurements) to generate cell density. For calculating recombination efficiency, 100 DCX cells were counted along the dorsoventral axis. These cells were then classified as positive or negative for tdTomato (in imaged mice), eYFP (in ChR2 mice) or GFP (in Arch mice). For the morphological analysis of immature neurons, z-stack images of tdTomato+ cells were traced and imported into Adobe Illustrator CS5 where neurons were reconstructed using the tracing tool. Images of the reconstructed neurons were opened in Fiji (<http://fiji.sc/Fiji>) where Sholl analysis was conducted using the Sholl analysis plug-in with parameters previously described (Sahay *et al*, 2011a). For calculating Ki67 number in implanted mice, six sections across the DV axis of each hemisphere DG (~400um between sections) were counted.

To sample the phenotypes of opsin/reporter positive cells in NestinCreER^{T2} mice, 35um sections were cut through the DG of *Nestin^{ChR2}* mice, and two sections/mouse (~1200 mm between sections, one dorsal and one medioventral section) were imaged by taking confocal stacks at 40x. To calculate the percentage of ChR2-eYFP⁺ cells that expressed Ki67, DCX or NeuN, the total eYFP⁺ cells in 300 um x 200 um region of interest in the upper blade of the DG were counted in the green channel, and then in the red channel the number of eYFP⁺ cells immunoreactive for DCX, Ki67 or NeuN was counted. Characterization of the ChR2-eYFP positive cells 6 weeks after induction by co-staining for developmental stage markers demonstrated that 12.1 \pm 0.4% (n = 3 mice) expressed Ki67 (i.e. were mitotic or recently mitotic), 52.2 \pm 2.5% (n = 4 mice) were DCX-positive (i.e. were proliferating progenitor cells, neuroblasts or immature, <3 week-old, neurons) and 67.7 \pm 4.1% (n = 3 mice) expressed NeuN (i.e. were neurons >2 weeks of age).

For assessing activity in the DG following window implantation, window implanted mice were placed in an open field box and allowed to explore for 20 min (as described below) and sacrificed 60 min after exploration. 50um sections were cut along the entire AP axis of the hippocampus, and every 6th section was stained for cFos and counts of cFos+ nuclei in the GCL were taken (dorsal DG).

Dentate gyrus granule cell imaging

In vivo 2-photon imaging:

We used the same imaging system as described previously (Kaifosh et al., 2013; Lovett-Barron et al., 2014), with the addition of an 8kHz resonant galvanometer (Bruker). Approximately 150-250 mW of laser power was used during imaging, with adjustments in power levels to accommodate varying window clarity. To optimize light

transmission, we adjusted the angle of the mouse's head using two goniometers (Edmund Optics, +/-10 degree range) such that the imaging window was parallel to the objective. All images were acquired with a Nikon 40X NIR water-immersion objective (0.8 NA, 3.5 mm WD) in distilled water. We continuously acquired red (tdTomato) and green (GCaMP6f) channels separated by an emission cube set (green, HQ525/70m-2p; red, HQ607/45m-2p; 575dcxr, Chroma Technology) at 1024 x 1024 pixels covering 300 μm x 300 μm at 15 Hz with photomultiplier tubes (green GCaMP fluorescence, GaAsP PMT, Hamamatsu Model 7422P-40; red tdTomato fluorescence, multi-alkali PMT, Hamamatsu R3896). A custom dual stage preamp (1.4 x 10⁵ dB, Bruker) was used to amplify signals prior to digitization.

Training:

Mice were water-restricted (>90% pre-deprivation weight) and trained to run on a cue-deplete burlap treadmill belt for water rewards over the course of 1-2 weeks. We applied a progressively restrictive water reward schedule, with mice initially receiving 40 randomly placed rewards per lap and ultimately receiving 3 randomly placed rewards per lap. Mice were trained for 20 minutes daily until they regularly ran at least one lap per minute. Mice were also habituated to the optical instrumentation (presence of objective, laser, shutter sounds) prior to imaging experiments.

Contexts:

Similar to our previous work, each context (1 and 2) consisted of the same treadmill belt (the same sequence of 3 joined fabric ribbons), but distinct in their visual, auditory, tactile, and olfactory stimuli (Fig 4A) (Lovett-Barron et al., 2014). During imaging sessions, mice received three randomly placed water rewards per lap, with reward positions changing randomly each lap. To allow for comparison of GC activity between similar contexts, the same three fabrics were used in the same order, but the locations of all of the tactile cues were shuffled between the two belts.

Stimulus presentation and behavioral readout:

Visual, auditory, and olfactory stimuli were presented and behavioral data were recorded as described previously (Kaifosh et al., 2013; Lovett-Barron et al., 2014). In order to reliably track the position of the treadmill belt, we established registration anchors at known positions along the belts and interpolated between them using a quadrature encoded movement signal tied to the rotation of the treadmill wheels. Registration anchors were marked by radio-frequency identification (RFID) buttons (16mm, 125kHz, SparkFun Electronics) at evenly spaced positions along the belt, and were read off as they passed over a fixed RFID reader (ID-12LA, SparkFun). The rotational quadrature signal was produced by marking treadmill wheels with offset tick marks, and this signal was encoded by a pair of photodiodes (SEN-0024, SparkFun) aligned to the wheels (<0.5cm resolution).

Calcium data processing:

All imaging data were analyzed using the SIMA software package (Kaifosh et al., 2014). Motion correction was performed using a 2D Hidden Markov Model (Dombeck et al., 2007; Kaifosh et al., 2013), with modifications to accommodate the specific features of data acquired with resonant galvanometers. These modifications have been made freely available with the latest versions of SIMA. Only the green GCaMP channel was used for estimating motion artifacts. In cases where motion artifacts were not adequately corrected, the affected data was discarded from further analysis. The especially sparse activity of dentate granule cells prevented the successful application of activity-based segmentation methods. Therefore, we used the SIMA project's ROI Buddy graphical user interface (Kaifosh et al., 2014) to draw regions of interest (ROIs) over GC somata visible in the time-averaged image of the motion-corrected green/GCaMP6f channel. We also used this software to determine the correspondence of ROIs across datasets from different trials in which the same FOV was imaged. To prevent the introduction of any bias, the red tdTomato channel was not viewed when drawing ROIs, but only referenced after all ROIs had been drawn in order to tag ROIs over tdTomato expressing cells as newborn GCs.

Dynamic GCaMP6f fluorescence signals were extracted from ROIs using SIMA according to the previously described formulation (Kaifosh et al., 2014). We then computed the relative fluorescence changes ($\Delta F/F$) (as described in (Jia et al., 2011)), with uniform smoothing window $t_1 = 3$ sec. and baseline size $t_2 = 60$ sec. We detected statistically significant calcium transients as described previously (Dombeck et al., 2007; Lovett-Barron et al., 2014). In order to improve our sensitivity, we then recalculated the baseline of the raw signal after masking

frames identified previously as occurring during a significant transient. $\Delta F/F$ was then recalculated, and transients re-estimated. Transients less than one second were removed to reduce false positives. This iterative procedure was repeated three times and effectively removed the transient contamination from the calculated baseline.

Spatial tuning vector and tuning specificity p-value analysis:

When evaluating the spatial tuning of GCs, we restricted our analysis to running-related epochs, defined as consecutive frames of forward locomotion (defined as an imaging frame in which at least one forward pair of beam breaks occurred) at least 1 sec in duration and with a minimum peak speed of 5 cm/sec. Consecutive epochs separated by < 0.5 seconds were merged. Running-related transients were defined as those that were initiated during a running-related epoch. Transient start was defined as the first imaging frame with mean fluorescence $\geq 2\sigma$, with σ equal to the standard deviation of the baseline frames. Offset was defined as the first frame with mean fluorescence $\leq 0.5\sigma$ (Dombeck et al. 2007). The spatial tuning vector was calculated as $\sum_j \frac{e^{i\theta_j}}{o(\theta_j)}$, where θ_j is the position of the mouse at the onset time of the j-th running-related transient, and o_j is the fraction of running frames acquired at position θ_j . In order to assess the significance of the spatial selectivity, for each cell we generated a null tuning distribution by shuffling the transient onset times (restricted to running frames) and repeatedly recomputing the tuning specificity. This process was repeated 100,000 times, and the p-value was defined as the fraction of this distribution that exceeded the GC's tuning specificity.

Spatial information p-value analysis:

For each cell we first computed the spatial information content (Skaggs, et al., 1993) as $I_N = \sum_{i=1}^N \lambda_i \ln \frac{\lambda_i}{\lambda} p_i$ where λ_i and p_i are the transient rate and fraction of time spent in the i th bin, λ is the overall firing rate, and N is the number of bins. We computed I_N for multiple values of $N = 2, 4, 5, 8, 10, 20, 25,$ and 100 . We then created 100,000 random reassignments of the transient onset times within the running-related epochs and re-computed the values of I_N^s , where s is the index of the shuffle. To roughly correct for biases in the calculation of mutual information, we then subtracted the mean of this null distribution from all estimates to obtain values $\hat{I}_N = I_N - \frac{1}{100,000} \sum_{s=1}^{100,000} I_N^s$. Finally, we computed a single estimate of the information content for the true transient onset times, $\hat{I} = \max_N \hat{I}_N$, and for the shuffles, $\hat{I}_s = \max_N \hat{I}_N^s$. The spatial tuning p-value was taken as the fraction of values of s for which \hat{I} exceeded \hat{I}_s .

Remapping analysis:

Rate maps were formed by dividing the number of transients starting in each bin by the occupancy of that bin. We calculated rate maps with 100 position bins and smoothed with a Gaussian kernel ($\sigma=3$ bins). The tuning curve correlation for each cell was defined as the Pearson correlation coefficient between tuning curves for a cell in the two sequential context exposures. The centroid shift for each cell was defined as the angle (in radians) between the tuning directions calculated for the two context exposures. For both metrics, the shuffle distributions were calculated by estimating the tuning curve correlations or tuning shifts when cells were paired by a sub-sampled Cartesian product of cell identities (1000 pairs per shuffle).

Behavioral testing

Optogenetic modulation

In Arch experiments, the patch cables were interfaced to an FC/PC rotary joint (Doric lenses), which was attached on the other end to a 593.5 nm laser diode that was controlled by a Master-8 stimulator (AMPI). During the light on epoch, yellow light was provided for the full 5 min at a light power of 10mw at the tip of the implanted fiber optic. For ChR2 experiments, the hardware configuration was identical to the Arch experiments with the exception that illumination was provided by a 473nm laser diode (OEM). During the light on epoch, mice received blue light illumination for the full 5 min at 10hz, 20 ms pulses at a light power of 8 mw at the tip of the implanted fiber.

Open field test

Mice were quickly attached to the fiber optic patch cables (bilaterally) via a zirconia sleeve, then placed in an open-field chamber 22.1" wide x 22.1" long x 15.83" high (Kinder Scientific) with high lux illumination (600lux). Sessions lasted for 15 min consisting of three 5 min epochs: light off, light on, and light off. Data was collected and analyzed with *MotorMonitor* software, and total distance traveled and percent of that distance traveled in the center of the arena was documented.

Elevated plus maze

Hardware configuration and experimental protocols for EPM were identical to OFT (15min session, 5min light off/on). Mice were placed in the closed arm of the open field and allowed to explore the maze. Sessions were videotaped, and the videos were analyzed for time spent in closed arms, open arms and center of the maze using *TopScan* software (Clever Sys).

Fear conditioning:

Hardware configuration and light intensity was identical to OFT and EPM, stimulation epochs are presented in the text. Different cohorts of mice were used for each test, thus littermate controls were used for each experiment to control for differences in genetic background. Conditioning took place in Coulbourn Instruments fear conditioning boxes that contained one clear plexiglass wall, three aluminum walls and a stainless steel grid as a floor. Mice were brought in to the testing room in a novel cage, attached to the fiber optic patch cables then placed in fear conditioning boxes. The training session began with the onset of the houselight and fan, and anise scent was placed under the grid floor. In this one-trial contextual fear conditioning protocol, mice received light stimulations as described in the text, and 180 s after placement of the mouse in the training context and onset of houselight and fan, mice received single 2-s foot shock of 0.75 mA. All freezing was measured before the single footshock. The mouse was taken out 15 s after termination of the foot shock and returned to its home cage. The grid and the waste tray were cleaned Sani-Cloths® HB Germicidal Disposable Wipes (Orangeburg, NY) between runs. Mice were recorded by digital video cameras mounted above the conditioning chamber, and were scored for freezing by an investigator blind to the genotype of the animal.

Contextual fear discrimination:

Conditioning took place in the same Coulbourn fear conditioning boxes as above. For training in context A mice were brought into the testing room in a novel cage with novel bedding on the floor. The training context (A) included a houselight and fan, and anise scent was placed under the grid floor. Mice were exposed to the context, then after 180s, they received single 2s foot shock of 0.75mA. Mice were taken out 15s after termination of the foot shock and returned to their home cage. The box was cleaned with Sanicloths between runs. For exposure to the similar (no-shock) context, B, mice were brought into the testing room in transport buckets by the same experimenter who had handled the mice for the training context. Context B shared many features of the training context, A, including an exposed stainless steel grid floor, but differed in that two plastic inserts were used to cover the walls and make them circular, the house fan and lights were turned off, and the chamber door was left ajar during testing. A lemon scent was used as an olfactory cue, and 70% ethanol was used to clean the grids between runs. Mice were run first in context B, then after 2h, mice were placed in the training context A. As the shock was given at the end of context A, all freezing in both contexts was assessed before animals were shocked. Measurement of the freezing levels (by an experimenter blind to treatment condition) in both the training context (3-min pre-shock) and the similar context (3min) each day allowed the assessment of freezing in the two contexts.

For the dissimilar context, C, the grid floor was covered with a plastic panel and cage bedding. The chamber walls were covered and made circular using plastic inserts, the house fan and lights were turned off, and a mild lemon scent was placed below the grid floor. The chamber door was left ajar during testing. 70% ethanol used to clean the chamber between runs. Mice were run first in context C, then after 2hr were run in context A. As above, the shock was given at the end of context A, ensuring that all freezing measured in both contexts was assessed before animals were shocked. Measurement of the freezing levels in both the training context (3-min pre-shock) and the novel context (3min) each day allowed the assessment of freezing in the two contexts.

Statistics

For all optogenetic behavioral data, data was analyzed using ANOVA with repeated measurements where appropriate. All tests are described in the appropriate figure legends. Group numbers were based on previous optogenetic and 2-photon imaging experiments (Kheirbek et al., 2013; Lovett-Barron et al., 2014). For imaging data, for all normally distributed data, a Welch's two-sample T-Test was used for comparison of means with $n-1$ degrees of freedom. The Mann-Whitney U Test was used for comparison of means in non-normally distributed data with $n-1$ degrees of freedom. A paired student's T-Test was used for comparison of means in paired data with $n-1$ degrees of freedom. The one-sided Kolmogorov-Smirnov (KS) test was used for testing the hypothesis that a distribution was drawn from an underlying theoretical distribution with $n-1$ degrees of freedom (uniformity in the case of Fig 2E and 4D). The two-sided two-sample Kolmogorov-Smirnov test with $n-1$ degrees of freedom was used for testing the null hypothesis that two empirical distributions were drawn from the same continuous underlying distribution.

Supplementary references

- Dombeck, D.A., Khabbaz, A.N., Collman, F., Adelman, T.L., and Tank, D.W. (2007). Imaging large-scale neural activity with cellular resolution in awake, mobile mice. *Neuron* *56*, 43-57
- Dranovsky, A., Picchini, A.M., Moadel, T., Sisti, A.C., Yamada, A., Kimura, S., Leonardo, E.D., and Hen, R. (2011). Experience dictates stem cell fate in the adult hippocampus. *Neuron* *70*, 908-923
- Jia, H., Rochefort, N.L., Chen, X., and Konnerth, A. (2011). In vivo two-photon imaging of sensory-evoked dendritic calcium signals in cortical neurons. *Nature protocols* *6*, 28-35
- Kaifosh, P., Lovett-Barron, M., Turi, G.F., Reardon, T.R., and Losonczy, A. (2013). Septo-hippocampal GABAergic signaling across multiple modalities in awake mice. *Nat Neurosci* *16*, 1182-1184
- Kaifosh, P., Zaremba, J.D., Danielson, N.B., and Losonczy, A. (2014). SIMA: Python software for analysis of dynamic fluorescence imaging data. *Frontiers in neuroinformatics* *8*, 80
- Kheirbek, M.A., Drew, L.J., Burghardt, N.S., Costantini, D.O., Tannenholz, L., Ahmari, S.E., Zeng, H., Fenton, A.A., and Hen, R. (2013). Differential control of learning and anxiety along the dorsoventral axis of the dentate gyrus. *Neuron* *77*, 955-968
- Kheirbek, M.A., Tannenholz, L., and Hen, R. (2012). NR2B-dependent plasticity of adult-born granule cells is necessary for context discrimination. *The Journal of neuroscience : the official journal of the Society for Neuroscience* *32*, 8696-8702
- Lovett-Barron, M., Kaifosh, P., Kheirbek, M.A., Danielson, N., Zaremba, J.D., Reardon, T.R., Turi, G.F., Hen, R., Zemelman, B.V., and Losonczy, A. (2014). Dendritic inhibition in the hippocampus supports fear learning. *Science* *343*, 857-863
- Madisen, L., Mao, T., Koch, H., Zhuo, J.M., Berenyi, A., Fujisawa, S., Hsu, Y.W., Garcia, A.J., 3rd, Gu, X., Zanella, S., *et al.* (2012). A toolbox of Cre-dependent optogenetic transgenic mice for light-induced activation and silencing. *Nat Neurosci* *15*, 793-802
- Madisen, L., Zwingman, T.A., Sunkin, S.M., Oh, S.W., Zariwala, H.A., Gu, H., Ng, L.L., Palmiter, R.D., Hawrylycz, M.J., Jones, A.R., *et al.* (2010). A robust and high-throughput Cre reporting and characterization system for the whole mouse brain. *Nat Neurosci* *13*, 133-140
- Sahay, A., Scobie, K.N., Hill, A.S., O'Carroll, C.M., Kheirbek, M.A., Burghardt, N.S., Fenton, A.A., Dranovsky, A., and Hen, R. (2011). Increasing adult hippocampal neurogenesis is sufficient to improve pattern separation. *Nature* *472*, 466-470